


## Number of populated electronic configurations in a hot dense plasma

Menahem Krief<sup>✉\*</sup>

*Racah Institute of Physics, The Hebrew University, 9190401 Jerusalem, Israel*

 (Received 20 December 2020; revised 27 February 2021; accepted 11 March 2021; published 26 March 2021)

In hot dense plasmas of intermediate or high- $Z$  elements in the state of local thermodynamic equilibrium, the number of electronic configurations contributing to key macroscopic quantities such as the spectral opacity and equation of state can be enormous. In this work we present systematic methods for the analysis of the number of relativistic electronic configurations in a plasma. While the combinatoric number of configurations can be huge even for mid- $Z$  elements, the number of configurations which have non-negligible population is much lower and depends strongly and nontrivially on temperature and density. We discuss two useful methods for the estimation of the number of populated configurations: (i) using an exact calculation of the total combinatoric number of configurations within superconfigurations in a converged super-transition-array (STA) calculation, and (ii) by using an estimate for the multidimensional width of the probability distribution for electronic population over bound shells, which is binomial if electron exchange and correlation effects are neglected. These methods are analyzed, and the mechanism which leads to the huge number of populated configurations is discussed in detail. Comprehensive average-atom finite-temperature density functional theory (DFT) calculations are performed in a wide range of temperature and density for several low-, mid-, and high- $Z$  plasmas. The effects of temperature and density on the number of populated configurations are discussed and explained.

DOI: [10.1103/PhysRevE.103.033206](https://doi.org/10.1103/PhysRevE.103.033206)

### I. INTRODUCTION

The calculation of radiative transport properties and equations of state from first principles are of key importance in the modeling of a wide variety of high energy density plasmas, which exist both in stellar interiors [1–11] and in terrestrial laboratories, such as  $Z$ -pinch and high-power laser facilities [12–20]. These macroscopic quantities entail a very sophisticated interplay between plasma physics and atomic physics.

In the calculation of spectral opacities, the bound-bound photoabsorption spectra results from all radiative transitions between all levels from all pairs of electronic configurations. In a hot dense plasma, the number of lines between each pair of configurations may be enormous [21,22] and statistical methods must be used. The unresolved-transition-array (UTA) method [23–26] treats all levels between each pair of configurations statistically, using analytic expressions for the energy moments of the transition array. In many cases, the number of configurations may also be extremely large and a such detailed-configuration-accounting (DCA) calculations are intractable as well. Similarly, in the calculation of equations of state, a huge number of electronic configurations should be taken into account, for an accurate calculation of the total partition function.

In this work we discuss in detail the number of electronic configurations in a hot dense plasma. The combinatoric number of possible configurations as well as the number of configurations which have a non-negligible population are examined. The combinatoric number of configurations is cal-

culated by using exact recursive relations [27]. Two methods for the estimation of the number of populated configurations are considered and compared. The calculations are performed in a very wide range of plasma temperature (100 eV–10 keV) and density ( $10^{-3}$ – $10^3$  g/cm<sup>3</sup>) for various low-, mid-, and high- $Z$  elements, using finite-temperature average-atom DFT calculations as well as super-transition-array (STA) calculations, employing the opacity code STAR [28,29]. The effects of temperature and density on the number of populated configurations are discussed and explained.

A relativistic electronic configuration  $C$  is defined by a set of occupation numbers  $\{q_s\}$  on relativistic  $s = (nlj)$  orbital shells, which are full solutions of the Dirac equation. In the statistical configuration approximation (neglecting the atomic structure within configurations [30,31]), the occupation of a configuration  $C$  is given by the Boltzmann distribution:

$$P_C = \frac{g_C e^{-(E_C - \mu Q_C)/k_B T}}{U_{tot}}, \quad (1)$$

where  $Q_C = \sum_s q_s$  is the number of bound electrons in  $C$ ,  $\mu$  is the chemical potential, the statistical weight of  $C$  is

$$g_C = \prod_s \binom{g_s}{q_s}, \quad (2)$$

where orbital degeneracy is  $g_s = 2j_s + 1$ , the total partition function is

$$U_{tot} = \sum_C g_C e^{-(E_C - \mu Q_C)/k_B T}, \quad (3)$$

\*menahem.krief@mail.huji.ac.il

and the the configuration average energy is

$$E_C = \sum_s q_s I_s + \frac{1}{2} \sum_{r,s} q_r (q_s - \delta_{rs}) H_{rs}, \quad (4)$$

where the residual energy is

$$I_s = \epsilon_s - \left\langle s \left| \frac{Z}{r} + V(r) \right| s \right\rangle, \quad (5)$$

where  $\epsilon_s$  is the orbital energy,  $V(r)$  is the self-consistent mean field central atomic potential, and  $H_{rs}$  is the average interaction energy of the two-electron configuration  $rs$ , given in terms of relativistic direct and exchange Slater integrals (explicit expressions can be found in Refs. [26,32,33]).

## II. COMBINATORIC NUMBER OF CONFIGURATIONS

First we demonstrate how to calculate the combinatoric number of configurations with  $Q$  electrons, which are distributed over a set of shells  $A = \{s_1 s_2 \cdots s_N\}$ , defined by

$$\mathcal{N}_Q^A = \sum_{\substack{\{q_s\}_{s=1}^N \\ \text{with } \sum_{s=1}^N q_s = Q}} 1,$$

where we have expressed the constraint that only configurations  $\{q_s\}_{s=1}^N$  with a total number of  $Q$  electrons are summed. This sum can be expressed in terms of partials sums over the population of the  $N$ th shell:

$$\mathcal{N}_Q^A = \sum_{q_N=0}^{\min(g_N, Q)} \sum_{\substack{\{q_s\}_{s=1}^{N-1} \\ \text{with } \sum_{s=1}^{N-1} q_s = Q - q_N}} 1. \quad (6)$$

Since the inner sum is actually  $\mathcal{N}_{Q-q_N}^{A/\{s_N\}}$ , where  $A/\{s_N\}$  denotes the set  $A$  excluding the shell  $s_N$ , we get the recursive relation

$$\mathcal{N}_Q^A = \sum_{q_N=0}^{\min(g_N, Q)} \mathcal{N}_{Q-q_N}^{A/\{s_N\}}. \quad (7)$$

We note that this recursion relation is performed simultaneously over the numbers of electrons  $Q$  and the number of shells  $N$ , and should obey the initial condition  $\mathcal{N}_Q^A = \delta_{Q,0}$  for an empty shell group  $A$ . The derivation above, which results from a simple combinatoric argument, can be proved by employing the powerful and general method of generating functions, as was done in detail Ref. [27], which deals with stable algorithms for the calculation of canonical partition functions, which were further generalized and improved in Refs. [34,35]. We note that in a recent work [36] an approach that leads to recurrence and analytic relations as well as a statistical modeling of the combinatoric number of configurations is developed in detail.

The total combinatoric number of configurations for an element with an atomic number  $Z$  is given by summing the number of configurations over all ionization levels:

$$\mathcal{N}_C^{\text{combin}} = \sum_{Q=0}^Z \mathcal{N}_Q^A, \quad (8)$$

where  $A$  is the set of all shells from which configurations are constructed. We note that, in general, the number of

bound shells is a function of the atomic number, temperature, and density, which determines the self-consistent central potential—for example, a higher- $Z$  element has a larger number of bound shells; due to the higher nucleus charge and a higher density plasma it may have a smaller number of shells due to an increased pressure ionization effect (bound states dissolving into the continuum [33,37–45]).

One can also define the number of configurations taking into account only charge states with probability larger than  $p$ :

$$\mathcal{N}_C^{\text{combin}}(p) = \sum_{Q, P_Q > p} \mathcal{N}_Q^A, \quad (9)$$

where the charge state distribution is given by the sum of probabilities of all configurations with a total charge  $Q$ :

$$P_Q = \sum_{C, Q_C=Q} P_C. \quad (10)$$

We note that Eq. (9) may depend strongly on the parameter  $p$ , and may give a severe overestimation for the number of *populated* configurations, since each charge state  $Q$  can correspond to a huge number of configurations, some of which have an extremely low probability. In addition, an exact computation of the ion charge distribution (10) [via Eq. (1)] is in many cases intractable, due the huge number of configurations that need to be taken into account. However, many approximated methods for the calculation of the charge state distribution in a plasma exist (for example, via the well known Saha equations) and can be used “externally” in the calculation of Eq. (9). In this work we will use a more accurate charge state distribution which is obtained from an STA calculation (see below).

## III. NUMBER CONFIGURATIONS WITHIN SUPERCONFIGURATIONS

In the STA method [28,33,46–53], a large number of configurations  $C$  are grouped into superconfigurations (SCs), commonly denoted by  $\Xi = \Pi_\sigma \sigma^{Q_\sigma}$ , which are defined as sets of configurations which have  $Q_\sigma$  electrons in each “supershell”  $\sigma$ , which is a group of shells. The total occupation of a super configuration is naturally

$$P_\Xi = \sum_{C \in \Xi} P_C, \quad (11)$$

and the combinatoric number of configurations within a superconfiguration is

$$\mathcal{N}_C(\Xi) = \sum_{C \in \Xi} 1. \quad (12)$$

As was already noted in Ref. [27],  $\mathcal{N}_C(\Xi)$  can be evaluated exactly, using the recursive relation (7). Since electron occupation numbers in different supershells are independent, Eq. (7) can be used for each supershell, to give the combinatoric number of configurations within a superconfiguration:

$$\mathcal{N}_C(\Xi) = \prod_\sigma \mathcal{N}_{Q_\sigma}^\sigma, \quad (13)$$

where  $\mathcal{N}_{Q_\sigma}^\sigma$  is calculated by applying the recursion relation (7) for each supershell.

A simple estimate for the number of populated configurations, is given by the number of configurations within all populated superconfigurations with a probability larger than  $p$ :

$$\mathcal{N}_C^{\text{in SCs}}(p) = \sum_{\Xi, P_{\Xi} > p} \mathcal{N}_C(\Xi). \quad (14)$$

where we have expressed the constraint that only superconfigurations with a non-negligible occupation are included.

We note that the combinatoric number of superconfigurations, for a given set of supershells, can also be calculated using the recursion relation (7), by treating the supershells  $\sigma$  as shells, defining  $A = \{\sigma_1 \cdots \sigma_N\}$ , with total degeneracies  $g_{\sigma} = \sum_{s \in \sigma} g_s$  and summing over all ionization levels.

#### IV. ESTIMATION OF THE NUMBER OF POPULATED CONFIGURATION

In this section we discuss a very simple way to estimate the number of populated configurations, without using a state-of-the-art sophisticated STA method, as was suggested in the previous section. This method was presented in the seminal book [54] and was used subsequently in Refs. [28,29]. In this method, only the bound shells and chemical potential are needed, so that the estimate for the number of populated configurations can be obtained, for example, by solving the Dirac equation in a Thomas-Fermi potential [55] or in a more advanced average-atom model potential [33,37–45].

Let us estimate the number of populated configurations. Neglecting the electron-electron interaction effects beyond the self-consistent field model, the configuration average energy given in Eq. (4) can be approximated as a first-order polynomial of the occupation numbers:

$$E_C \approx \sum_s q_s \epsilon_s. \quad (15)$$

Under this approximation, the total partition function is

$$U_{\text{tot}} = \prod_s (1 + e^{-(\epsilon_s - \mu)/k_B T})^{g_s}, \quad (16)$$

and the configuration probability (1) becomes a simple multivariate binomial distribution of the occupation numbers  $\{q_s\}$ , given by

$$P(\{q_s\}) \equiv P_C = \prod_s \binom{g_s}{q_s} n_s^{q_s} (1 - n_s)^{g_s - q_s}, \quad (17)$$

where  $n_s = 1/(e^{(\epsilon_s - \mu)/k_B T} + 1)$  is the Fermi-Dirac distribution. The variance of the population of each shell is given by

$$\delta q_s \equiv \sqrt{\langle (q_s - \langle q_s \rangle)^2 \rangle} = \sqrt{g_s n_s (1 - n_s)}. \quad (18)$$

As illustrated in Figs. 1 and 2, it is evident that the occupation of shells whose energies are near the Fermi-Dirac step, which is located around  $-k_B T \lesssim \epsilon_s - \mu \lesssim k_B T$ , fluctuate, while the other shells are either filled or empty. These fluctuating shells may have a wide range of possibilities to distribute electrons over the magnetic quantum numbers  $0 \leq m_s \leq g_s$ . The fluctuating occupation numbers may give rise the a huge number of populated configurations, which increases exponentially with the number of fluctuating shells.

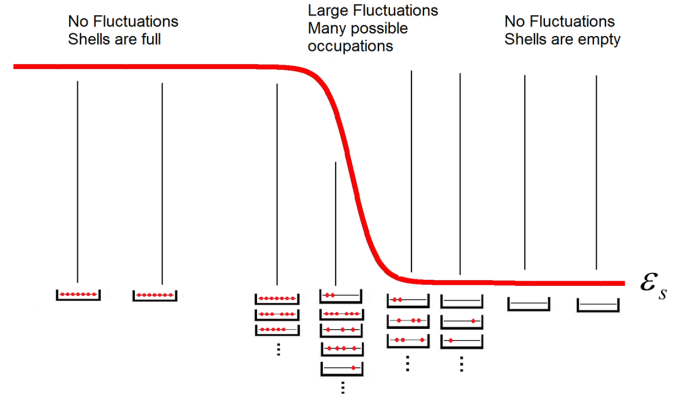


FIG. 1. A schematic description of the population of electrons over shells according to the Fermi-Dirac distribution (red thick line). The occupation of electronic shells which have energies nearby the Fermi-Dirac step (which is located at  $\epsilon_s \approx \mu$  and has a width of the order of  $k_B T$ ), fluctuate and result in wide range of possibilities to distribute electrons over the magnetic quantum numbers, while shells which are far from the Fermi-Dirac step are either filled or empty. The fluctuating occupation numbers may give rise to a huge number of populated electronic configurations.

The number of populated configurations can be estimated as the number of possibilities to put electrons in each shell, within a few standard deviations  $\delta q_s$  around the average occupation  $\langle q_s \rangle = g_s n_s$  of the multivariate distribution (17). The number of possible occupation numbers for each shell is estimated as  $\alpha \times \delta q_s$ , where  $\alpha/2$  is the number of standard deviations. Therefore, the number of populated configurations can be estimated by

$$\mathcal{N}_C^{\text{approx}} = \prod_s (\alpha \delta q_s + 1), \quad (19)$$

which is simply the multidimensional “width” of the multivariate binomial distribution ((17)).

We note that the result may depend on the somewhat arbitrary value chosen for  $\alpha$ , but it can be expected that a reasonable value should be in the range  $2 \lesssim \alpha/2 \lesssim 4$ , corresponding to a range of two to four standard deviations for the occupation of each shell. In order to demonstrate this,  $\mathcal{N}_C^{\text{approx}}$  was calculated as a function of  $\alpha$  in the range  $1 \leq \alpha \leq 10$  and compared with the number of configurations within populated superconfigurations [Eq. (14)] of a converged STA calculation. Two cases are considered: (1) iron ( $Z = 26$ ) at typical conditions of the recent Sandia Z experiments [12,15], with temperature  $T = 182$  eV and density  $\rho = 0.13$  g/cm<sup>3</sup>, and (2) gold ( $Z = 79$ ) with temperature  $T = 200$  eV and density  $\rho = 0.1$  g/cm<sup>3</sup>. The calculations were performed using the relativistic average-atom model implemented in the STA code STAR [3,26,28,29,31,43,51]. The number of bound shells was limited to a principle atomic number of  $n_{\text{max}} = 8$  (which corresponds to 64 relativistic orbitals), since highly excited bound orbitals can be accounted for by using the method detailed in Ref. [56], and therefore need not be accounted in the estimation of the number of populated configurations that are used in the calculation of spectral opacities. Illustration of the bound orbitals and the Fermi-Dirac step for the two cases is given Fig. 2. The supershell structure for each case

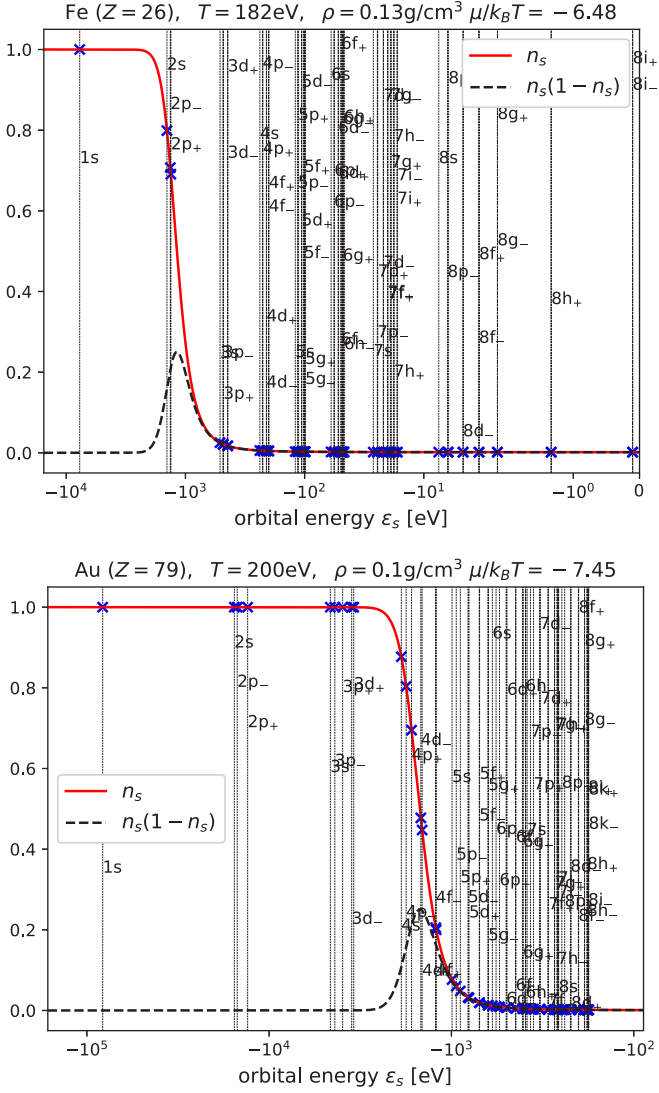


FIG. 2. The Fermi-Dirac distribution (red solid lines, as illustrated in Fig. 1) and the occupation fluctuation  $\delta q_s^2/g_s$  [black dashed lines, see Eq. (18)] as a function of orbital energy, for iron at  $T = 182$  eV,  $\rho = 0.13$  g/cm<sup>3</sup> (upper figure) and gold at  $T = 200$  eV,  $\rho = 0.1$  g/cm<sup>3</sup> (lower figure). The relativistic Dirac bound orbitals are listed and represented as vertical dashed thin lines at their appropriate bound energies. The resulting chemical potential is given in the title.

are given in Tables I and II. In Fig. 3 we present the number of populated configurations as a function of  $\alpha$ , in comparison to the combinatoric number of configurations over all ionization levels [Eq. (8)] and over all ionization levels with occupation probabilities larger than  $10^{-2}$ ,  $10^{-4}$ ,  $10^{-5}$ , and  $10^{-6}$  [Eq. (9)] as well as the number of configurations within populated superconfigurations [Eq. (14)], with occupation probabilities larger than  $10^{-6}$ ,  $10^{-7}$ , and  $10^{-8}$ . These results are also given explicitly in Table III. The strong dependence on  $\alpha$  is evident, and it seems, as expected, that a good choice is  $\alpha = 6$ , which corresponds to 3 standard deviations for the occupation of each shell.

It is evident that the probability thresholds affect the resulting number of configurations by about 1–2 orders of

TABLE I. The converged relativistic supershell structure (left column) for iron at  $T = 182$  eV,  $\rho = 0.13$  g/cm<sup>3</sup>. The range for the number of electrons in each supershell (middle column), chosen such that the superconfiguration occupation is larger than  $10^{-7}$ , as well as the total supershell degeneracy (right column), are also given. The total number of superconfigurations is  $\mathcal{N}_{\Xi} = 2880$ .

Supershell $\sigma$	$Q_{\sigma}$ range	Degeneracy $g_{\sigma}$
(1s)	[2,2]	2
(2s)	[0,2]	2
(2p <sub>-</sub> )	[0,2]	2
(2p <sub>+</sub> )	[0,4]	4
(3s...5f <sub>-</sub> )	[0,7]	74
(5f <sub>+</sub> ...8i <sub>+</sub> )	[0,7]	294

magnitude, which is a reasonable accuracy for the number of configurations, which can be of the order of  $10^{15}$ – $10^{40}$ . It is evident that for the iron case the results for  $\mathcal{N}_C^{\text{combin}}(p)$  and  $\mathcal{N}_C^{\text{in SCs}}(p)$  agree to within 1–2 orders of magnitude. However, it is evident that for the gold case the  $\mathcal{N}_C^{\text{combin}}(p)$  values give a severe overestimation (by about ten orders of magnitude) compared to  $\mathcal{N}_C^{\text{in SCs}}(p)$ , which represents the correct estimate for the number of configurations that need to be taken into account in opacity calculations. As mentioned in Sec. II, this is to be expected since each charge state  $Q$  can correspond to a huge number of configurations, some of which have extremely low probabilities. This is more likely to happen for a high- $Z$  element, for which the supershell structure (see Table II) gives rise to only a small fraction of all possible configurations for some charge states. In this way  $\mathcal{N}_C^{\text{in SCs}}$  only accounts for configurations with non-negligible probabilities while  $\mathcal{N}_C^{\text{combin}}(p)$  accounts for all configurations for non-negligible charge states, without taking into account the confrontational structure [which determines the configuration probability in Eq. (1)].

Figure 4 shows the charge state distributions, which were obtained from converged STA calculations, together with the combinatoric number of configurations as a function of the number of bound electrons [Eq. (7)], for the iron and gold cases. The exponential growth for the combinatoric number of configurations for large values of bound electrons is evident, as expected. We note that the number of configurations in Eq. (9) is obtained by summing the number of configurations

TABLE II. Same as Table I, for gold at  $T = 200$  eV,  $\rho = 0.1$  g/cm<sup>3</sup>. The total number of superconfigurations is  $\mathcal{N}_{\Xi} = 10400$ .

Supershell $\sigma$	$Q_{\sigma}$ range	Degeneracy $g_{\sigma}$
(1s)	[2,2]	2
(2s)	[2,2]	2
(2p <sub>-</sub> )	[2,2]	2
(2p <sub>+</sub> )	[4,4]	4
(3s3p...3p <sub>+</sub> )	[7,8]	8
(3d...3d <sub>+</sub> )	[9,10]	10
(4s...4f <sub>+</sub> )	[3,27]	32
(5s...7d <sub>+</sub> )	[0,12]	140
(7f <sub>-</sub> ...8k <sub>+</sub> )	[0,7]	208

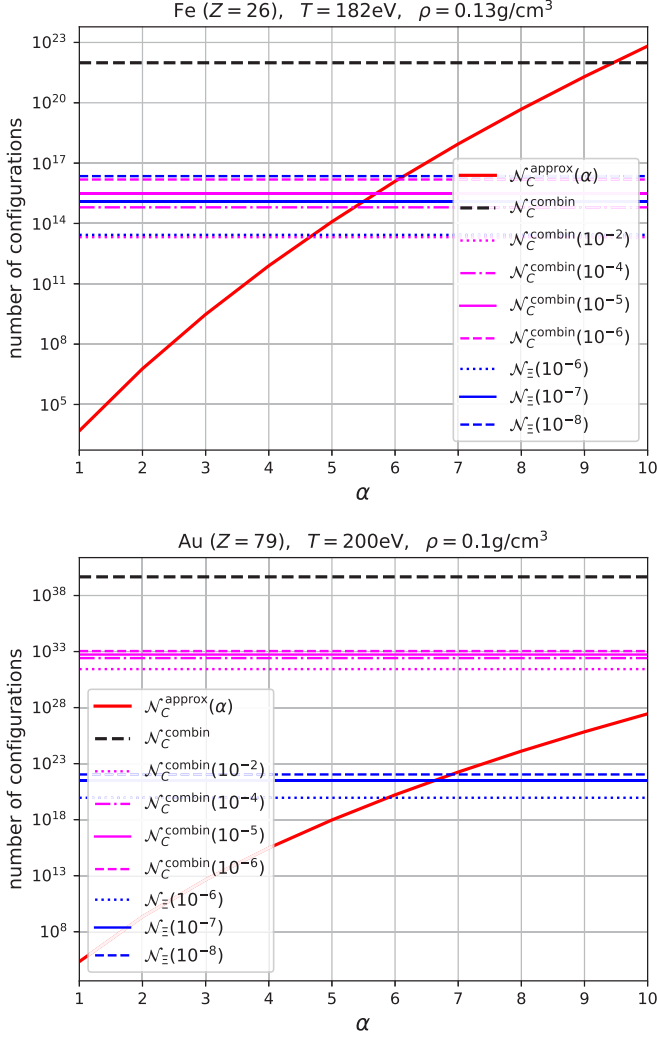


FIG. 3. The estimate given in Eq. (19) for the number of populated configurations, as a function of the parameter  $\alpha$  (red solid lines), for iron at  $T = 182$  eV,  $\rho = 0.13$  g/cm<sup>3</sup> (upper figure) and gold at  $T = 200$  eV,  $\rho = 0.1$  g/cm<sup>3</sup> (lower figure). Also shown are the combinatoric number of configurations over all ionization levels [Eq. (8), black dashed lines] and over all ionization levels with probabilities larger than  $10^{-2}$ ,  $10^{-4}$ ,  $10^{-5}$ , and  $10^{-6}$  respectively [Eq. (9), magenta lines], as well as the number of configurations within populated superconfigurations [Eq. (14)], with probabilities larger than  $10^{-6}$ ,  $10^{-7}$ , and  $10^{-8}$ , respectively [Eq. (14), blue lines].

TABLE III. Various values for the number of configurations for the two cases shown in Fig. 3.

	Fe, $T = 182$ eV, $\rho = 0.13$ g/cm <sup>3</sup>	Au, $T = 200$ eV, $\rho = 0.1$ g/cm <sup>3</sup>
$\mathcal{N}_C^{\text{combin}}$	$9.78 \times 10^{21}$	$4.64 \times 10^{39}$
$\mathcal{N}_C^{\text{combin}}(10^{-2})$	$2.08 \times 10^{13}$	$2.71 \times 10^{31}$
$\mathcal{N}_C^{\text{combin}}(10^{-4})$	$6.34 \times 10^{14}$	$2.6 \times 10^{32}$
$\mathcal{N}_C^{\text{combin}}(10^{-5})$	$3.2 \times 10^{15}$	$5.39 \times 10^{32}$
$\mathcal{N}_C^{\text{combin}}(10^{-6})$	$1.53 \times 10^{16}$	$1.1 \times 10^{33}$
$\mathcal{N}_C^{\text{in SCs}}(10^{-6})$	$2.71 \times 10^{13}$	$9.01 \times 10^{19}$
$\mathcal{N}_C^{\text{in SCs}}(10^{-7})$	$1.22 \times 10^{15}$	$3.35 \times 10^{21}$
$\mathcal{N}_C^{\text{in SCs}}(10^{-8})$	$2.26 \times 10^{16}$	$1.1 \times 10^{22}$
$\mathcal{N}_C^{\text{approx}}(\alpha = 6)$	$1.25 \times 10^{16}$	$1.63 \times 10^{20}$

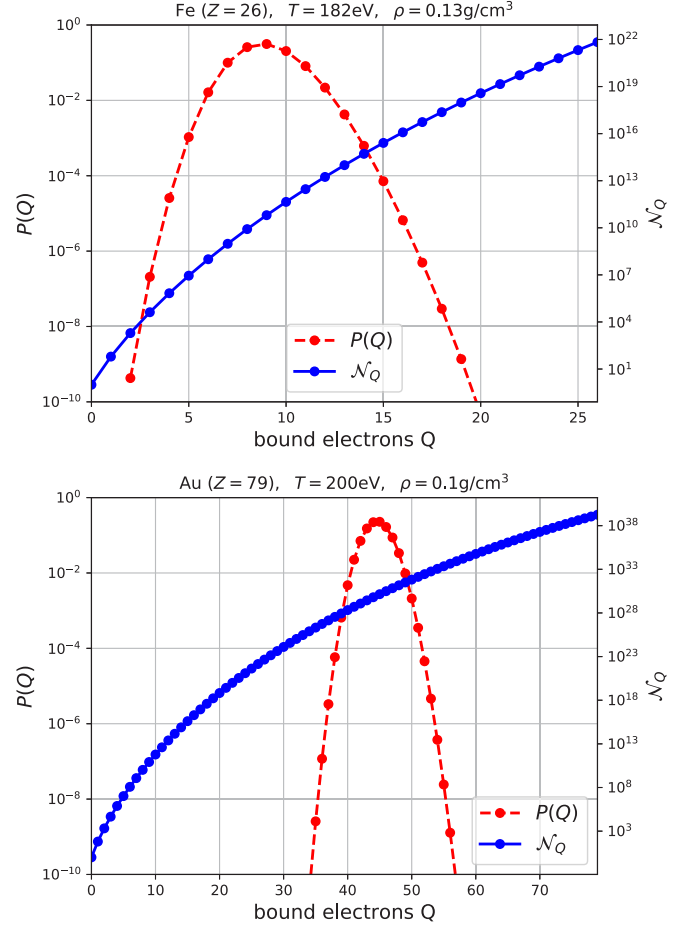


FIG. 4. The charge state distribution calculated using an STA model (red dashed lines, left axis) and the combinatoric number of configurations for each charge state [Eq. (8), blue lines, on the right axis], for iron at  $T = 182$  eV,  $\rho = 0.13$  g/cm<sup>3</sup> (upper figure) and gold at  $T = 200$  eV,  $\rho = 0.1$  g/cm<sup>3</sup> (lower figure).

per charge state in Fig. 4 in the overlapping range with the charge state distribution.

Finally, we note that it is possible to overcome the binomial approximation (17) using the correlated probability formalism. In Ref. [57] electron-electron interactions are taken into account in the screening constant model which is applicable for small interactions. The resulting correlation coefficients are calculated to second order in the interaction energy. As noted by Perrot and Blenski in Ref. [58], this method is complicated to implement in practice and performs poorly for low temperatures. Perrot and Blenski introduced in Ref. [58] a simple method, which overcomes these difficulties by replacing the binomial distribution with its correlated Gaussian continuous limit, which is applicable for orbital shells with large degeneracy and which are not close to being full or empty. As was shown in Ref. [59], this approximation is accurate to less than 1%. Hence, by using this Gaussian approximation in order to calculate the population variance of shells with a large degeneracy and which are not close to being full or empty, and the binomial approximation for the remaining shells (as was done above), can give a better approximation for the number of configurations, which takes

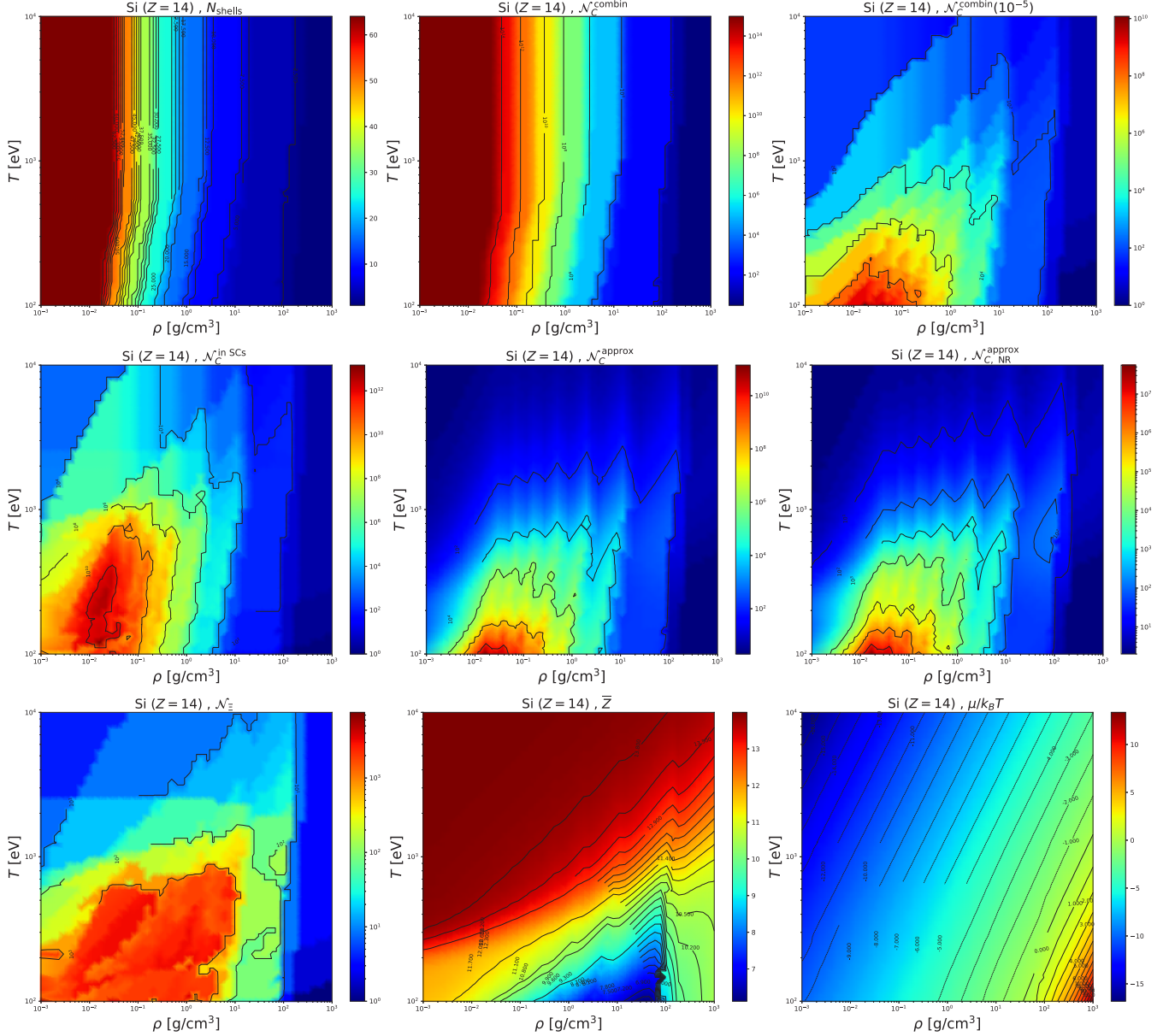


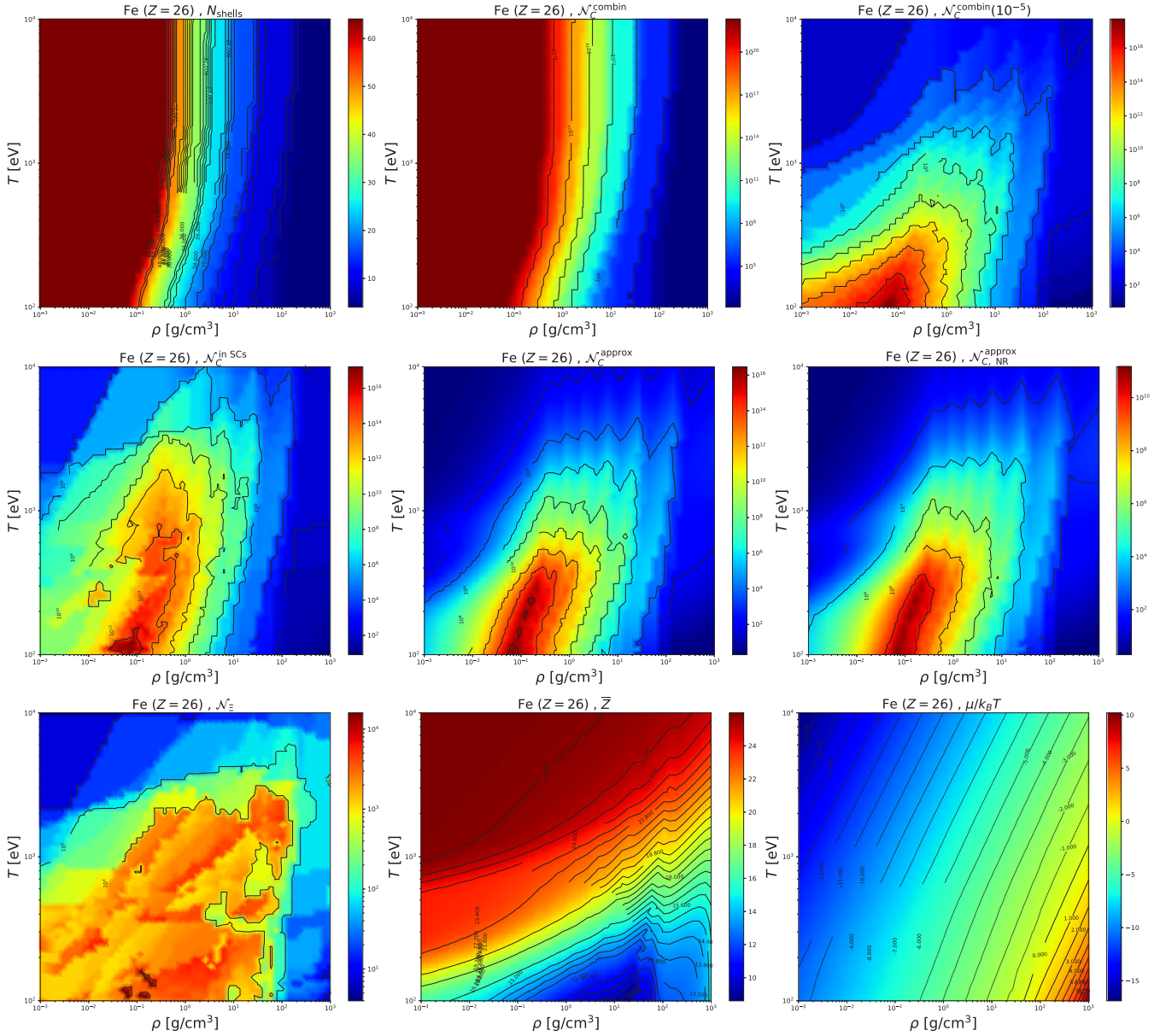
FIG. 5. Various color plots for silicone ( $Z = 14$ ), as a function of temperature and density (left to right, top to bottom): the number of bound shells  $N_{\text{shells}}$ , the combinatoric number of relativistic configurations  $\mathcal{N}_C^{\text{combin}}$  over all ionization levels [Eq. (8)] and over all ionization levels with probability larger than  $10^{-5}$  [Eq. (9)], the number of superconfigurations in a converged STA calculation  $\mathcal{N}_C^{\text{SCs}}$ , the number of configurations within superconfigurations  $\mathcal{N}_C^{\text{in SCs}}$  [Eq. (14)] with  $p = 10^{-7}$ , approximated number of populated relativistic  $\mathcal{N}_C^{\text{approx}}$  and nonrelativistic  $\mathcal{N}_C^{\text{approx,NR}}$  configurations, the average ionization  $\bar{Z}$ , and the normalized chemical potential  $\mu/k_B T$ .

into account electron-electron interactions. However, this is beyond the scope of this paper, and will be performed in a future work.

## V. RESULTS

Detailed finite temperature density functional theory (DFT) calculations in the spherical average-atom approximation [33,37–45] followed by STA calculations using the atomic code STAR [28,29], were performed over a wide range of plasma temperatures, 100 eV–10 keV, and densities,  $10^{-3}$ – $10^3$  g/cm<sup>3</sup>, for the following low-, mid-, and high- $Z$  elements: silicone ( $Z = 14$ ), iron ( $Z = 26$ ), xenon ( $Z = 54$ ), and

gold ( $Z = 79$ ). The results are shown in Figs. 5–8, and include the average ionization, the chemical potential, the number of bound shells, the combinatoric number of configurations over all ionization levels [Eq. (8)] and over all ionization levels with probabilities larger than  $10^{-5}$  [Eq. (9); the charge distribution was obtained from the STA calculations], the number of populated superconfigurations in the converged STA calculation, the number of configurations within these superconfigurations, and the approximated number of relativistic and nonrelativistic populated configurations. First, it is evident that, as expected, the number of configurations grows exponentially with the atomic number. It is seen that even for mid- $Z$  plasmas the number of populated configurations can


 FIG. 6. Same as Fig. 5, for iron ( $Z = 26$ ).

be huge (larger than  $10^{13}$ ) in a wide range of temperature and density, and a detailed configuration accounting (DCA) calculation may be extremely costly, while a full detailed-line-accounting (DLA) calculation is probably impossible. For a higher- $Z$  plasma such as xenon and gold, there is a wide range of temperature and density with a populated number of configurations larger than  $10^{20}$ , which is completely intractable for a DCA calculation, and highlights the need for an STA [28,33,46–48,50–52] or average-atom [60–62] method for opacity calculations.

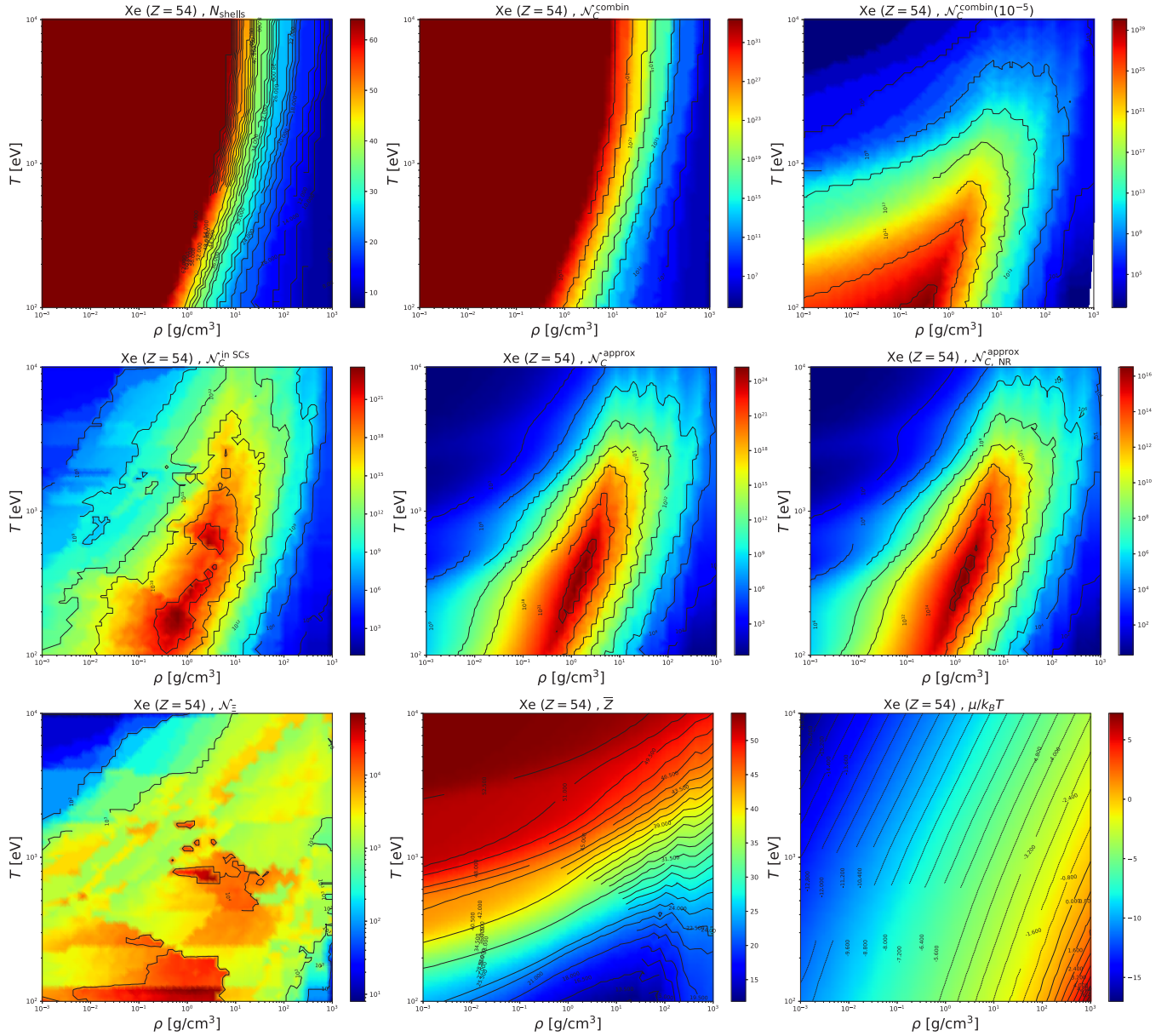
A comparison of the number of configurations within superconfigurations,  $\mathcal{N}_C^{\text{in SCs}}$ , and approximated number of populated relativistic configurations,  $\mathcal{N}_C^{\text{approx}}$ , shows a good qualitative and even quantitative agreement, which proves that  $\mathcal{N}_C^{\text{approx}}$  is a very good simple estimate for the number of populated configurations. In addition, the plots for the number of superconfigurations  $\mathcal{N}_{\pm}$  in a converged STA

calculation in comparison the the number of populated configurations highlights the strength of the STA method: a computationally tractable number of superconfigurations (in the range of  $10^3$ – $10^5$ ), which may contain a huge number of configurations (more than  $10^{25}$  in some cases), yields a converged opacity calculation which would have been completely prohibitive in a configuration-based DCA calculation.

It is seen that the  $\mu/k_B T$  contours are approximately straight lines (when the density and temperatures are plotted on a logarithmic scale), a fact which agrees with the ideal gas result,

$$\mu_{\text{ideal}} = k_B T \ln(\Lambda^3 \bar{n}), \quad (20)$$

where  $\bar{n}$  is the number density and  $\Lambda = (2\pi\hbar^2/mk_B T)^{1/2}$  is the thermal wavelength, so that, in the thermodynamic range

FIG. 7. Same as Fig. 5, for xenon ( $Z = 54$ ).

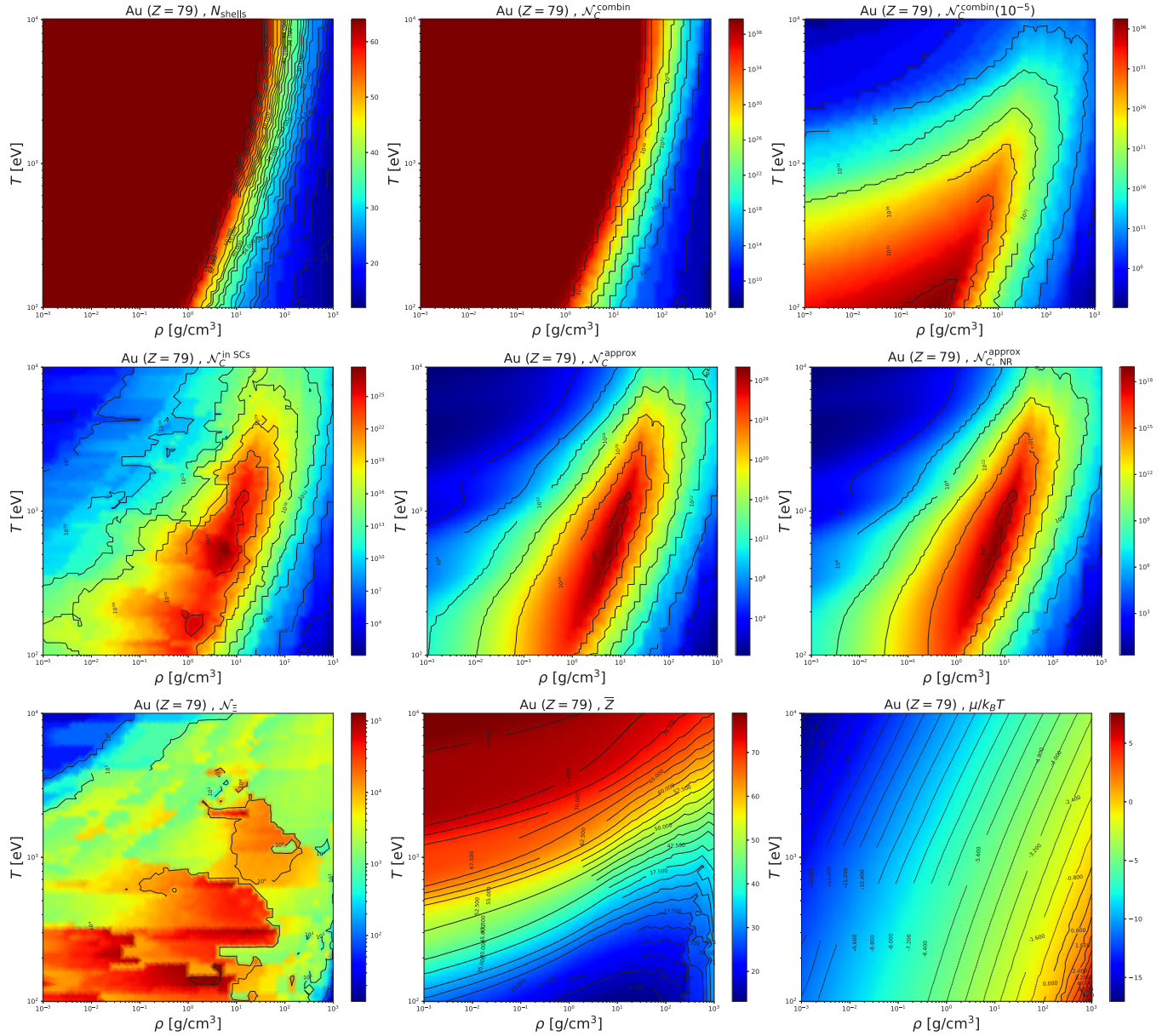
studied here, the chemical potential is a decreasing function of temperature and an increasing function of density, as shown in Figs. 9 and 10.

It is also evident from Figs. 5–8 that the combinatoric number of configurations over all ionization levels correlates perfectly with the number of bound shells that exists in the atomic potential. This is to be expected since this number of configurations depends on temperature and density only through the number of existing bound shells, and not on their properties (i.e., bound energies, wave functions, etc). As was explained in the previous section, since we are concerned in the number of configurations which should be taken into account in opacity calculations, the number of bound shells is limited here to 64, which results in a sharp front in the plots for the combinatoric number of configurations. It is also evident that  $\mathcal{N}_C^{\text{combin}}(p = 10^{-5})$  has a better agreement with  $\mathcal{N}_C^{\text{in SCs}}$  and  $\mathcal{N}_C^{\text{approx}}$  for the lower- $Z$  elements and for cases

with a smaller number of bound orbitals. As was discussed in the previous section, this is to be expected, since, as opposed to the superconfiguration accounting approach, the charge probability distribution does not contain information about the configuration structure and as a result some charge states may contain a huge amount of very low probability configurations, which are taken into account in Eq. (9).

Next, we discuss the temperature and density behavior for the populated number of configurations. As expected, it is seen in Figs. 5–8 that the number of populated configurations has a maximum as a function of temperature and density. For low temperatures, most shells have energies  $\epsilon_s < \mu$  and are therefore “frozen” either full or empty (see Fig. 1), while for moderate temperatures (which are different for each element and density) the Fermi-Dirac distribution has a shape of a step function, but with a finite width which allows large fluctuations for the occupation numbers of shells with energies




 FIG. 8. Same as Fig. 5, for gold ( $Z = 79$ ).

near the step (see Fig. 9). For higher temperatures, on the one hand, more shells are ionized, which results in a decrease in the number of populated configurations, and on the other hand the number of bound shells can be larger, due to a wider spatial extent of the atomic central potential, which reduces the effect of pressure ionization, as seen in the plots of the number of bound shells. The latter effect results in the slightly tilted maxima for the number of populated configurations as a function of temperature and density, seen in Figs. 5–8. In addition, it is evident that for low densities the number of populated configurations is small due to the decrease in the chemical potential (see Fig. 10), which reduces the number of fluctuating shells, while for very high densities most shells are pressure ionized (as seen in the plots of the number of bound shells) and those which are not are occupied and frozen, which leads again to a small number of populated configurations.

## VI. SUMMARY

Two useful methods for the estimation of the number of populated configurations in a hot dense plasma were studied. In the first method, an exact calculation of the total combinatoric number of configurations within superconfigurations in a converged super-transition-array (STA) calculation was used. In the second method, electron exchange and correlation effects are neglected, leading to a multivariate binomial distribution for the electronic occupation numbers, whose multidimensional width is an approximation for the number of populated configurations. The mechanism which leads to the huge number of populated configurations—namely, the fluctuations of electronic occupation numbers of bound shells nearby the Fermi-Dirac step—is demonstrated and discussed in detail. Comprehensive average-atom finite temperature DFT calculations are performed in a wide range of

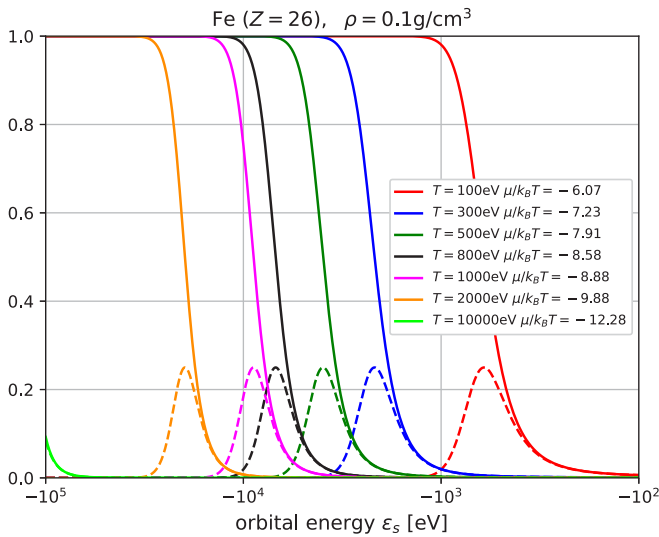


FIG. 9. The Fermi-Dirac distribution (solid lines) and the occupation fluctuation  $\delta q_s^2/g_s$  [dashed lines, see Eq. (18)] as a function of orbital energy, for iron at  $\rho = 0.1 \text{ g/cm}^3$ , and different temperatures in the range  $10^2$ – $10^4 \text{ eV}$  (lines are arranged from right to left).

temperature and density for several low-, mid-, and high- $Z$  plasmas, showing a good agreement between these two methods. In addition, the temperature and density dependence is discussed and explained.

The second method is much more simple than the first: only the bound shells and chemical potential are needed, so that the estimate for the number of populated configurations can be obtained, for example, by solving the Dirac equation in a Thomas-Fermi potential or in a more advanced average-atom model potential. This simple estimate can be very useful in

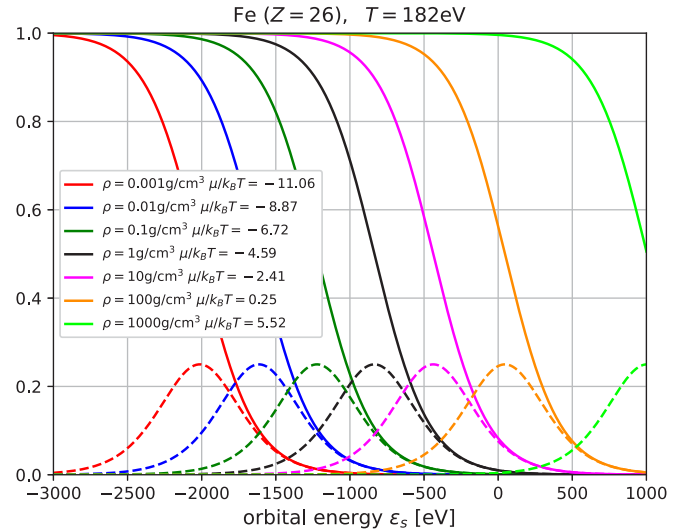


FIG. 10. The Fermi-Dirac distribution (solid lines) and the occupation fluctuation  $\delta q_s^2/g_s$  [dashed lines, see Eq. (18)] as a function of orbital energy, for iron at  $T = 182 \text{ eV}$ , and different densities in the range  $10^{-3}$ – $10^3 \text{ g/cm}^3$  (lines are arranged from left to right).

order to assess the computational ability to perform configuration based, or even line based opacity and equation of state calculations.

#### ACKNOWLEDGMENTS

We thank the anonymous referees for useful suggestions and comments, and, in particular, for suggesting the examination of the number of configurations with respect to probability thresholds and a discussion of possible improvements of the binomial approximation.

- [1] J. Christensen-Dalsgaard, M. Pia Di Mauro, G. Houdek, and F. Pijpers, On the opacity change required to compensate for the revised solar composition, *Astron. Astrophys.* **494**, 205 (2009).
- [2] F. L. Villante and A. M. Serenelli, A quantitative analysis of the solar composition problem, *Phys. Procedia* **61**, 366 (2015).
- [3] M. Krief, A. Feigel, and D. Gazit, Line broadening and the solar opacity problem, *Astrophys. J.* **824**, 98 (2016).
- [4] C. Mendoza, Computation of atomic astrophysical opacities, *Atoms* **6**, 28 (2018).
- [5] J.-C. Pain, F. Gilleron, and M. Comet, Detailed opacity calculations for astrophysical applications, *Atoms* **5**, 22 (2017).
- [6] C. J. Fontes, C. L. Fryer, A. L. Hungerford, P. Hakel, J. Colgan, D. P. Kilcrease, and M. E. Sherrill, Relativistic opacities for astrophysical applications, *High Energy Density Phys.* **16**, 53 (2015).
- [7] C. J. Fontes, H. L. Zhang, J. Abdallah, Jr., R. E. H. Clark, D. P. Kilcrease, J. Colgan, R. T. Cunningham, P. Hakel, N. H. Magee, and M. E. Sherrill, The Los Alamos suite of relativistic atomic physics codes, *J. Phys. B: At. Mol. Opt. Phys.* **48**, 144014 (2015).
- [8] J. Colgan, D. P. Kilcrease, N. H. Magee, M. E. Sherrill, J. Abdallah Jr., P. Hakel, C. J. Fontes, J. A. Guzik, and K. A. Mussack, A new generation of los alamos opacity tables, *Astrophys. J.* **817**, 116 (2016).
- [9] C. A. Iglesias, Iron-group opacities for B stars, *Mon. Not. R. Astron. Soc.* **450**, 2 (2015).
- [10] C. A. Iglesias and F. J. Rogers, Updated OPAL opacities, *Astrophys. J.* **464**, 943 (1996).
- [11] N. R. Badnell, M. A. Bautista, K. Butler, F. Delahaye, C. Mendoza, P. Palmeri, C. J. Zeippen, and M. J. Seaton, Updated opacities from the opacity project, *Mon. Not. R. Astron. Soc.* **360**, 458 (2005).
- [12] J. E. Bailey, T. Nagayama, G. P. Loisel, G. A. Rochau, C. Blancard, J. Colgan, Ph. Cosse, G. Faussurier, C. J. Fontes, F. Gilleron *et al.*, A higher-than-predicted measurement of iron opacity at solar interior temperatures, *Nature (London)* **517**, 56 (2015).
- [13] T. Nagayama, J. E. Bailey, G. Loisel, G. A. Rochau, J. J. MacFarlane, and I. Golovkin, Calibrated simulations of  $Z$  opacity experiments that reproduce the experimentally measured plasma conditions, *Phys. Rev. E* **93**, 023202 (2016).
- [14] T. Nagayama, J. E. Bailey, G. Loisel, G. A. Rochau, S. B. Hansen, C. Blancard, P. Cosse, G. Faussurier, F. Gilleron, J.-C. Pain *et al.*, Model uncertainties of local-thermodynamic

- equilibrium K-shell spectroscopy, *High Energy Density Phys.* **20**, 17 (2016).
- [15] T. Nagayama, J. E. Bailey, G. P. Loisel, G. S. Dunham, G. A. Rochau, C. Blancard, J. Colgan, P. Cosse, G. Faussurier, C. J. Fontes, F. Gilleron, S. B. Hansen, C. A. Iglesias, I. E. Golovkin, D. P. Kilcrease, J. J. MacFarlane, R. C. Mancini, R. M. More, C. Orban, J. C. Pain *et al.*, Systematic Study of *L*-Shell Opacity at Stellar Interior Temperatures, *Phys. Rev. Lett.* **122**, 235001 (2019).
- [16] C. A. Back, J. D. Bauer, O. L. Landen, R. E. Turner, B. F. Lasinski, J. H. Hammer, M. D. Rosen, L. J. Suter, and W. H. Hsing, Detailed Measurements of a Diffusive Supersonic Wave in a Radiatively Heated Foam, *Phys. Rev. Lett.* **84**, 274 (2000).
- [17] C. L. Fryer, E. Dodd, W. Even, C. J. Fontes, C. Greeff, A. Hungerford, J. Kline, K. Mussack, I. Tregillis, J. B. Workman *et al.*, Uncertainties in radiation flow experiments, *High Energy Density Phys.* **18**, 45 (2016).
- [18] A. S. Moore, T. M. Guymmer, J. Morton, B. Williams, J. L. Kline, N. Bazin, C. Bentley, S. Allan, K. Brent, A. J. Comley *et al.*, Characterization of supersonic radiation diffusion waves, *J. Quant. Spectrosc. Radiat. Transfer* **159**, 19 (2015).
- [19] N. Fleurot, C. Cavailler, and J. L. Bourgade, The Laser Mega-joule (LMJ) Project dedicated to inertial confinement fusion: Development and construction status, *Fusion Eng. Des.* **74**, 147 (2005).
- [20] C. Decker, R. E. Turner, O. L. Landen, L. J. Suter, P. Amendt, H. N. Kornblum, B. A. Hammel, T. J. Murphy, J. Wallace, N. D. Delamater, P. Gobby, A. A. Hauer, G. R. Magelssen, J. A. Oertel, J. Knauer, F. J. Marshall, D. Bradley, W. Seka, and J. M. Soures, Hohraum Radiation Drive Measurements on the Omega Laser, *Phys. Rev. Lett.* **79**, 1491 (1997).
- [21] H. A. Scott and S. B. Hansen, Advances in NLTE modeling for integrated simulations, *High Energy Density Phys.* **6**, 39 (2010).
- [22] F. Gilleron and J.-C. Pain, Efficient methods for calculating the number of states, levels and lines in atomic configurations, *High Energy Density Phys.* **5**, 320 (2009).
- [23] S. A. Moszkowski, On the energy distribution of terms and line arrays in atomic spectra, *Prog. Theor. Phys.* **28**, 1 (1962).
- [24] C. Bauche-Arnoult, J. Bauche, and M. Klapisch, Variance of the distributions of energy levels and of the transition arrays in atomic spectra, *Phys. Rev. A* **20**, 2424 (1979).
- [25] J. Bauche, C. Bauche-Arnoult, and M. Klapisch, Transition arrays in the spectra of ionized atoms, *Adv. At. Mol. Phys.* **23**, 131 (1988).
- [26] M. Krief and A. Feigel, Variance and shift of transition arrays for electric and magnetic multipole transitions, *High Energy Density Phys.* **17**, 254 (2015).
- [27] F. Gilleron and J.-C. Pain, Stable method for the calculation of partition functions in the superconfiguration approach, *Phys. Rev. E* **69**, 056117 (2004).
- [28] M. Krief, A. Feigel, and D. Gazit, Solar opacity calculations using the super-transition-array method, *Astrophys. J.* **821**, 45 (2016).
- [29] M. Krief, A. Feigel, and D. Gazit, A new implementation of the STA method for the calculation of opacities of local thermodynamic equilibrium plasmas, *Atoms* **6**, 35 (2018).
- [30] F. Gilleron, J.-C. Pain, Q. Porcherot, J. Bauche, and C. Bauche-Arnoult, Corrections to statistical modeling of spectra for plasmas at moderate or low temperatures, *High Energy Density Phys.* **7**, 277 (2011).
- [31] M. Krief and A. Feigel, The effect of first order superconfiguration energies on the opacity of hot dense matter, *High Energy Density Phys.* **15**, 59 (2015).
- [32] A. Bar-Shalom, J. Oreg, and W. H. Goldstein, Effect of configuration widths on the spectra of local thermodynamic equilibrium plasmas, *Phys. Rev. E* **51**, 4882 (1995).
- [33] A. A. Ovechkin, P. A. Loboda, V. G. Novikov, A. S. Grushin, and A. D. Solomyannaya, RESEOS—a model of thermodynamic and optical properties of hot and warm dense matter, *High Energy Density Phys.* **13**, 20 (2014).
- [34] B. G. Wilson, F. Gilleron, and J.-C. Pain, Further stable methods for the calculation of partition functions in the superconfiguration approach, *Phys. Rev. E* **76**, 032103 (2007).
- [35] J.-C. Pain, F. Gilleron, and B. G. Wilson, Optimized recursion relation for the computation of partition functions in the superconfiguration approach, *High Energy Density Phys.* **37**, 100891 (2020).
- [36] J.-C. Pain and M. Poirier, Analytical and numerical expressions for the number of atomic configurations contained in a super-shell, *J. Phys. B: At. Mol. Opt. Phys.* **53**, 115002 (2020).
- [37] D. A. Liberman, Self-consistent field model for condensed matter, *Phys. Rev. B* **20**, 4981 (1979).
- [38] B. F. Rozsnyai, Relativistic Hartree-Fock-Slater calculations for arbitrary temperature and matter density, *Phys. Rev. A* **5**, 1137 (1972).
- [39] T. Blenski and K. Ishikawa, Pressure ionization in the spherical ion-cell model of dense plasmas and a pressure formula in the relativistic pauli approximation, *Phys. Rev. E* **51**, 4869 (1995).
- [40] B. Wilson, V. Sonnad, P. Sterne, and W. Isaacs, PURGATORIO—a new implementation of the INFERNO algorithm, *J. Quant. Spectrosc. Radiat. Transfer* **99**, 658 (2006).
- [41] V. G. Novikov and A. A. Ovechkin, Calculations of the equation of state by the Liberman model, *Math. Models Comput. Simul.* **3**, 290 (2011).
- [42] A. A. Ovechkin, P. A. Loboda, and A. L. Falkov, Plasma opacity calculations using the Starrett and Saumon average-atom model with ion correlations, *High Energy Density Phys.* **30**, 29 (2019).
- [43] M. Krief, Y. Kurzweil, A. Feigel, and D. Gazit, The effect of ionic correlations on radiative properties in the solar interior and terrestrial experiments, *Astrophys. J.* **856**, 135 (2018).
- [44] N. M. Gill and C. E. Starrett, Tartarus: A relativistic green's function quantum average atom code, *High Energy Density Phys.* **24**, 33 (2017).
- [45] C. E. Starrett, N. M. Gill, T. Sjoström, and C. W. Greeff, Wide ranging equation of state with Tartarus: A hybrid green's function/orbital based average atom code, *Comput. Phys. Commun.* **235**, 50 (2019).
- [46] A. Bar-Shalom, J. Oreg, W. H. Goldstein, D. Shvarts, and A. Zigler, Super-transition-arrays: A model for the spectral analysis of hot, dense plasma, *Phys. Rev. A* **40**, 3183 (1989).
- [47] T. Blenski, A. Grimaldi, and F. Perrot, A superconfiguration code based on the local density approximation, *J. Quant. Spectrosc. Radiat. Transfer* **65**, 91 (2000).
- [48] G. Hazak and Y. Kurzweil, A Configurationally-Resolved-Super-Transition-Arrays method for calculation of the spectral absorption coefficient in hot plasmas, *High Energy Density Phys.* **8**, 290 (2012).
- [49] Y. Kurzweil and G. Hazak, Summation of the spectra of all partially resolved transition arrays in a supertransition array, *Phys. Rev. E* **94**, 053210 (2016).

- [50] B. G. Wilson, C. A. Iglesias, and M. H. Chen, Partially resolved super transition array method, *High Energy Density Phys.* **14**, 67 (2015).
- [51] M. Krief and D. Gazit, Star: A new STA code for the calculation of solar opacities, in *Workshop on Astrophysical Opacities*, Astronomical Society of the Pacific Conference Series Vol. 515 (ASP, San Francisco, 2018), p. 63.
- [52] J. Bauche, C. Bauche-Arnoult, and O. Peyrusse, *Atomic Properties in Hot Plasmas: From Levels to Superconfigurations* (Springer, Berlin, 2015).
- [53] J.-C. Pain, Super transition arrays: A tool for studying spectral properties of hot plasmas, *Plasma* **4**, 42 (2021).
- [54] A. F. Nikiforov, V. G. Novikov, and V. B. Uvarov, *Quantum-Statistical Models of Hot Dense Matter: Methods for Computation Opacity and Equation of State*, Progress in Mathematical Physics Vol. 37, (Birkhäuser, Basel, 2005).
- [55] R. P. Feynman, N. Metropolis, and E. Teller, Equations of state of elements based on the generalized Fermi-Thomas theory, *Phys. Rev.* **75**, 1561 (1949).
- [56] J.-C. Pain and F. Gilleron, Accounting for highly excited states in detailed opacity calculations, *High Energy Density Phys.* **15**, 30 (2015).
- [57] J. M. Green, The statistical mechanics of the interdependent electrons in the screening constant model of the many-electron-atom, *J. Quant. Spectrosc. Radiat. Transfer* **4**, 639 (1964).
- [58] F. Perrot and T. Blenski, Electronic structure and statistical mechanics of ionic configurations in hot plasmas, *J. Phys. IV (France)* **10**, 473 (2000).
- [59] B. G. Wilson, Evaluating orbital occupation number correlations in high-temperature plasmas, *J. Quant. Spectrosc. Radiat. Transfer* **49**, 241 (1993).
- [60] D. Shalitin, J. Stein, and A. Ron, Level and line broadening for Thomas-Fermi atoms at finite temperature, *Phys. Rev. A* **29**, 2789 (1984).
- [61] J. Stein, D. Shalitin, and A. Ron, Average-atom models of line broadening in hot dense plasmas, *Phys. Rev. A* **31**, 446 (1985).
- [62] B. F. Rozsnyai, Solar opacities, *J. Quant. Spectrosc. Radiat. Transfer* **71**, 655 (2001).